crystals

MDPI

Article

Temperature-Dependent Optical Properties of Graphene on Si and SiO_2/Si Substrates

Sisi Wu [1], Lingyu Wan [1,*], Liangmin Wei [1], Devki N. Talwar [2], Kaiyan He [1] and Zhechuan Feng [1]

[1] Center on Nanoenergy Research, Laboratory of Optoelectronic Materials & Detection Technology, Guangxi Key Laboratory for the Relativistic Astrophysics, School of Physical Science & Technology, Guangxi University, Nanning 530004, China; 1907301087@st.gxu.edu.cn (S.W.); lmwei19@163.com (L.W.); gredhky@gxu.edu.cn (K.H.); fengzc@gxu.edu.cn (Z.F.)

[2] Department of Physics, University of North Florida, Jacksonville, FL 32224, USA; d.talwar@unf.edu

* Correspondence: LYW2017@gxu.edu.cn

Abstract: Systematic investigations are performed to understand the temperature-dependent optical properties of graphene on Si and SiO_2/Si substrates by using a variable angle spectroscopic ellipsometry. The optical constants of graphene have revealed changes with the substrate and temperature. While the optical refractive index (n) of monolayer graphene on Si exhibited clear anomalous dispersions in the visible and near-infrared region (400–1200 nm), the modification is moderate for graphene on SiO_2/Si substrate. Two graphene sheets have shown a pronounced absorption in the ultraviolet region with peak position related to the Van Hove singularity in the density of states. By increasing the temperature from 300 K to 500 K, for monolayer graphene on Si, the n value is gradually increased while k decreased. However, the optical constants [n, k] of monolayer graphene on SiO_2/Si exhibited unpredictable wave variations. In the wavelength range of 400–1200 nm, an experiential formula of a like-Sellmeier equation is found well suited for describing the dispersions of graphene on Si and SiO_2/Si substrates.

Keywords: graphene; spectroscopic ellipsometry; optical properties; temperature-dependent characteristics

Citation: Wu, S.; Wan, L.; Wei, L.; Talwar, D.N.; He, K.; Feng, Z. Temperature-Dependent Optical Properties of Graphene on Si and SiO_2/Si Substrates. *Crystals* **2021**, *11*, 358. https://doi.org/10.3390/cryst11040358

Academic Editor: Giuseppe Prestopino

Received: 7 February 2021
Accepted: 26 March 2021
Published: 29 March 2021

1. Introduction

Since the seminal experimental realization of one atom thick graphene sheets [1] along with the measurements of quantum Hall effect [2], a great deal of interest has emerged in both the fundamental research and the development of device engineering concepts. Graphene has an extremely high carrier mobility ~15,000 $cm^2\ V^{-1}\ S^{-1}$ [3] and thermal conductivity 5000 $W\ m^{-1}\ K^{-1}$ [4] with a very strong Young's modulus ~1 TPa [5]. The Dirac Fermions in graphene has caused both integer and fractional quantum Hall effect [6]. Unconventional superconductivity has also been realized in a 2-dimensional superlattice created by stacking two sheets of twisted graphene relative to each other by a small angle [7,8]. Along with the unique electronic features, graphene has displayed extraordinary optical responses. Graphene, being a one-atom-thick sheet of carbon exhibits significant absorption in the visible to infrared wavelength region (2.3%) with reflectance less than 0.1% [9]. This means that a one-atom-thick graphene layer is extremely transparent having a high degree of flexibility with excellent optical properties.

As the variety of graphene for commercial applications is intensifying, so does the compulsion for scientists to exploit reliable characterization methods for studying basic properties and for engineers to design optoelectronic devices for achieving optimum performance. To assess the optical traits of graphene, several measurements have been performed using spinning-disc Picometrology (SDP), spectroscopic ellipsometry (SE), and transmission spectroscopy, etc. [10–27]. For graphene SiO_2/Si wafer, the complex refractive index is measured earlier by SDP at 532 nm and 633 nm [10]. Optical constants of graphene

have also been extracted by SE measurements [11–25]. However, the existing results of optical behavior for graphene are significantly different. The difference in outcomes is linked either to the methods used for preparing graphene samples with different numbers of layers and/or substrates.

This work aimed to understand the optical and temperature-dependent features of commercial graphene. A series of graphene samples were prepared by ACS Material, LLC using standard manufacturing procedures (product detail found on the website of https://www.acsmaterial.com/graphene-on-silicon-substrate.html accessed on 29 March 2021). Graphene was first prepared on copper foil by the chemical vapor deposition (CVD) method and then transferred onto Si and on SiO_2/Si substrates. The graphene qualities are examined through Raman spectroscopy and atomic force microscopy (AFM). The temperature-dependent optical properties are systemically investigated by exploiting a variable angle spectroscopic ellipsometry (VASE) method. The refractive index (n) and extinction coefficient (k) of the graphene sheets having different layers prepared on Si and SiO_2/Si substrates are carefully analyzed, establishing temperature-dependence between 300 K and 500 K. The anomalous optical dispersions of graphene prepared on Si and SiO_2/Si in the visible to near-infrared wavelength region (i.e., λ between 400 to 1200 nm), are well described by a modified Sellmeier equation.

2. Materials and Methods

Four graphene samples were meticulously examined by using VASE and variable temperature methods. The samples considered here were: (a) monolayer and bilayer graphene on Si substrate, and (b) monolayer, bilayer graphene on SiO_2/Si substrate (a Si wafer covered with a 300 nm SiO_2 layer). The dimensions of the graphene sheets were 2.54 cm × 2.54 cm. To examine the graphene qualities, room temperature Raman scattering spectra were measured using a micro-region Raman spectrometer with an excitation laser source of a wavelength of 532 nm and a spot size of 2 μm (iHR550, HORIBA, Kyoto, Japan), and the surface morphology of the samples were examined by the atomic force microscope (Dimension Icon, BRUKER NANO Inc., Billerica, MA, USA). The SE measurements were performed by using a Müeller Matrix Ellipsometer (Wuhan Eoptics Technology Co. Ltd., Wuhan, China) equipped with a heating and cooling system (THMS600, Linkam, Surrey, UK). The optical constants were extracted by modeling and data fitting analysis. The SE has the advantages of being a non-destructive and highly accurate technique. In the VASE studies, we used deuterium and halogen sources and varied the incident angles from 50°, 55°, 60°, 65°, and 70°, respectively. The beam size was about 4 mm. To study the temperature-dependent characteristics of graphene, we recorded the angle of polarization psi (ψ) and phase difference delta (Δ) of the reflective polarization lights between 300–500 K in the steps of 20 K.

To extract the optical constants, we fitted and modeled the recorded data of psi (ψ) and delta (Δ) by using Eometrics (Wuhan Eoptics Technology Co. Ltd., Wuhan, China). In our data analysis, a three-layer model was adopted, which properly included contributions from the substrate, oxide layer, and graphene, and the goodness of fitting was evaluated by the Mean Squared Error (MSE) method. Since the manufacturing procedures would induce a modification of bandgap properties of graphene [28–31], the dispersion properties of the graphene layers were described by 5 Tauc-Lorentz oscillators and 1 Drude oscillator. As for the oxide layer (SiO_2) and the substrate (Si), their dispersions were described by the Sellmeier and parametric models which were provided by the materials database of Eometrics.

3. Results and Discussion

3.1. Raman Scattering and AFM Measurements

Raman spectroscopy was used to characterize the quality of the transferred graphene. Figure 1 shows the room temperature Raman scattering spectra recorded for four graphene samples, in which all samples displayed typical Raman peaks of graphene. All graphene

samples included two intrinsic Raman peaks (G, 2D) and two disorder-induced peaks (D, D+D″ peaks for graphene on Si, and D, D′+D″ peaks for graphene on SiO_2) [32–34]. Among the defect-activated peaks, D′+D″ and D+D″ corresponded to the combination mode of the D′ and D″ modes as well as the D and D″ modes [34]. Si had strong absorption in the visible wavelength, the intensity of Raman scattering light for the graphene on Si substrate was weaker than that of graphene on SiO_2/Si substrate. The Raman scattering results indicated there existed a degree of defects in the four transferred graphene sheets. The intensity ratio between the 2D band and the G band can determine the number of graphene layers [35–37]. The I_{2D}/I_G values were higher than 2, in the range between 1 and 2, and lower than 1, corresponding to the presence of monolayer graphene, bilayer graphene, and three or more layers, respectively [35]. As for our four graphene samples, the I_{2D}/I_G values of two monolayer graphene were respectively 2.1 (on Si substrate) and 3.4 (on SiO_2/Si substrate) while those of two bilayer graphene were 1.5 (on Si substrate) and 1.7 (SiO_2 /Si substrate).

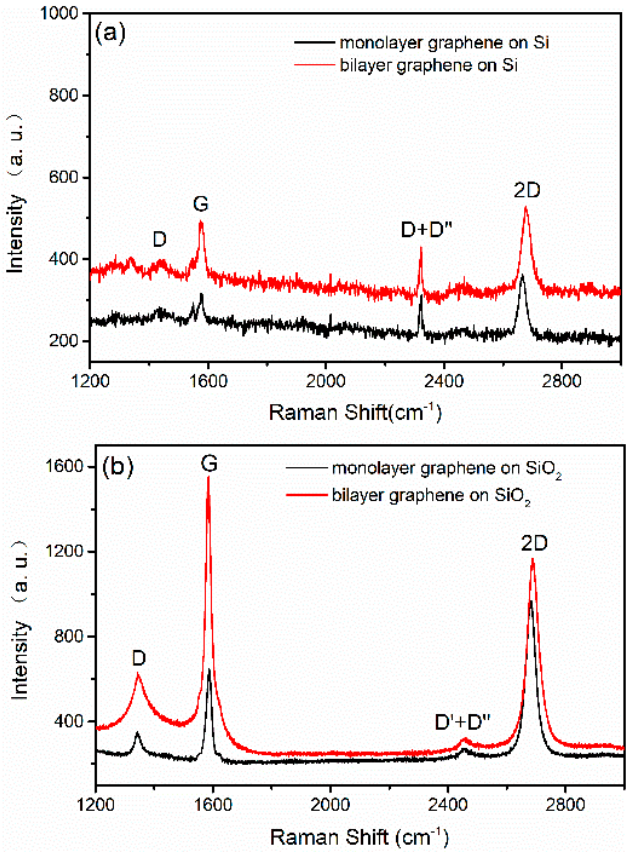

Figure 1. Raman scattering spectra of graphene samples. (**a**) graphene on Si substrate; (**b**) graphene on SiO_2/Si substrate.

Figure 2 illustrates the AFM images of graphene samples displaying smooth surfaces with a few surface contaminants. In 2 μm × 2 μm AFM images, the Root Mean Square (RMS) roughness was around 1.5–4.5 nm and the average roughness was 0.6–0.9 nm respectively. The samples had enough smooth surfaces for SE measurements and analysis.

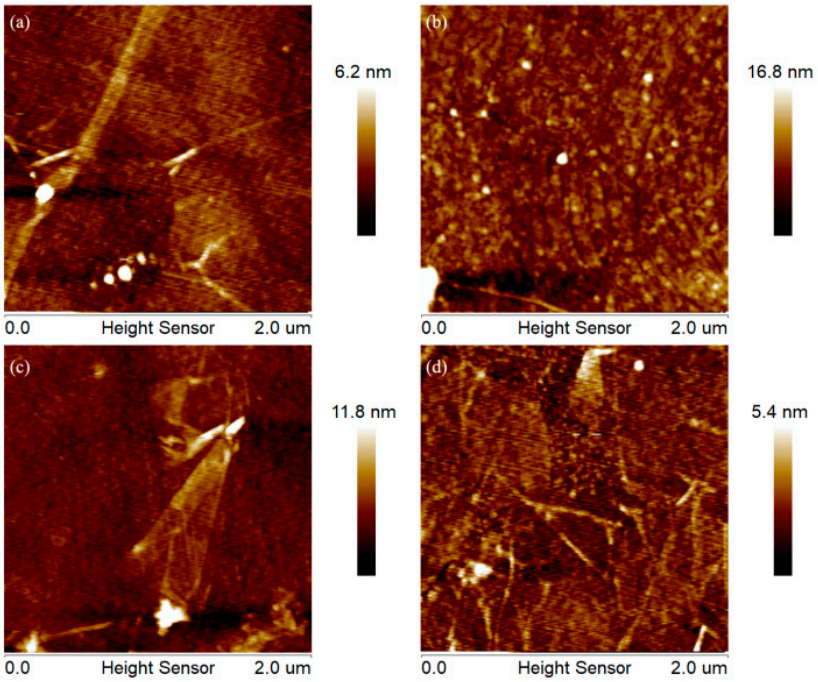

Figure 2. Atomic force microscopy (AFM) images of graphene samples. (**a**) monolayer graphene on Si substrate; (**b**) bilayer graphene on Si substrate; (**c**) monolayer graphene on SiO_2 substrate; (**d**) bilayer graphene on SiO_2 substrate.

3.2. Spectroscopic Ellipsometric Measurements

The optical characteristics of graphene samples were investigated by variable angle spectroscopic ellipsometry. In Figure 3a–d we have displayed the measured psi(ψ) and delta(Δ) at 300 K for monolayer graphene samples on Si and SiO_2/Si substrates, respectively by varying incident angles from 50°, 55°, 60°, 65°, and 70°. The experimental data (black solid lines) and the fitted curves (red dotted lines) compared reasonably well. In Table 1, for four samples the thicknesses of graphene and oxide layers and the MSE values are presented. The low MSE values (<15 in Table 1) indicated good fits. The thicknesses of monolayer graphene on Si and on SiO_2/Si were 0.38 nm and 0.34 nm, respectively, which was in accordance with those previously reported [13,16,21,25]. In Table 2, the fitting parameters of Tauc-Lorentz and Drude oscillators for monolayer graphene on Si and SiO_2/Si substrates are presented, where Amp_n, Br_n, Eo_n, and Eg_n correspond to amplitude, broadening, center energy, and bandgap energy of oscillator n (n is an integer), and Scat. Time is scattering time, respectively. The bandgap energy of Tauc-Lorentz oscillators as shown in Table 2 well agreed with the reports in References [28–31], indicating the dispersion models for graphene layers we have chosen were reasonable.

The extracted optical constants (n and k) in the wavelength range of 218–1200 nm are shown in Figure 3e,f. It is to be noted that graphene sheets on Si and on SiO_2/Si exhibited markedly different optical properties. In the range of λ between 400–1200 nm, the monolayer graphene on Si exhibited anomalous dispersions with a larger extinction coefficient than those on SiO_2/Si. In the ultraviolet wavelength range λ between 220–400 nm, the n of monolayer graphene on Si displayed a sharp peak while on SiO_2/Si it revealed a moderate feature. Likewise, the k of monolayer graphene on Si exhibited a pronounced peak at ~4.64 eV while a weak peak was noticed at ~4.78 eV for graphene on SiO_2/Si. The peak position of k, which is considered as a van Hove singularity of graphene density of state [11], showed an energy difference of 0.14 eV for two samples. Obviously, the interaction of graphene with substrate had significantly affected the optical properties of graphene.

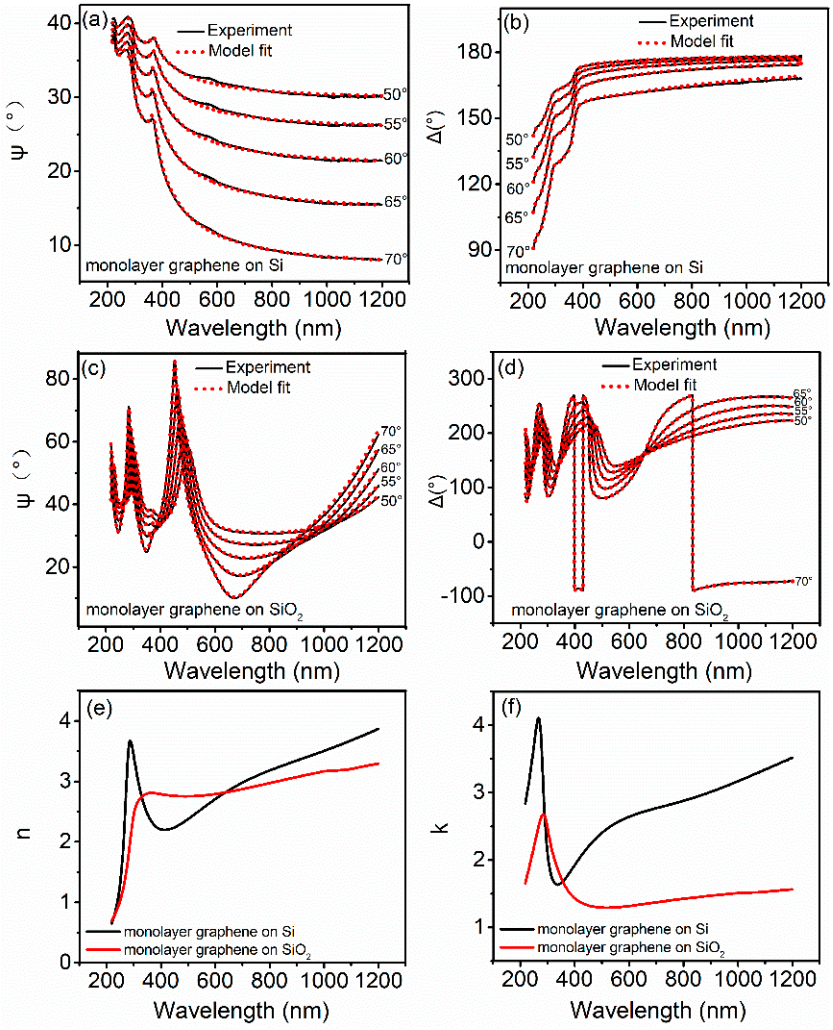

Figure 3. Variable angle spectroscopic ellipsometry of graphene on Si and on SiO_2/Si substrates at room temperature. the measured (black line) and fitting (red dot) psi(ψ) and delta(Δ) spectra for the monolayer graphene on Si substrate (**a**,**b**) and on SiO_2/Si substrate (**c**,**d**), (**e**,**f**) represent the extracted refractive indices (n) and the extinction coefficients (k) by SE fitting.

Table 1. Thicknesses and mean squared error (MSE) values of graphene samples.

Samples		1 Layer on Si	2 Layers on Si	1 Layer on SiO_2/Si	2 Layers on SiO_2/Si
Thickness (nm)	Graphene	0.380 ± 0.002	0.730 ± 0.005	0.340 ± 0.001	0.880 ± 0.001
	Oxide Layer	4.560 ± 0.004	4.700 ± 0.008	297.980 ± 0.011	293.370 ± 0.011
MSE		4.252	4.868	11.564	13.498

Moreover, we compared the optical constants of monolayer and bilayer graphene. In Figure 4 the optical constants extracted by SE measurements are displayed for four graphene samples along with the fitted results. We noticed that for graphene samples on Si substrate, the n decreased while k increased with the increase in the number of layers. Moreover, the peak positions of k were found redshifted. This was possibly due to the increase of the number of layers—the layer-to-layer interaction decreased the energy of π-to-π^* exciton transition near the M point of the Brillouin zone [38,39]. Unlike graphene on Si, the bilayer graphene on SiO_2/Si displayed a greater n than that of monolayer graphene as wavelengths were longer than 600 nm. Moreover, it exhibited significant dispersion features compared to the monolayer graphene on SiO_2/Si. It has been suggested earlier that

the substrates modulate the dispersion of graphene sheets and the enhanced layer-to-layer interaction of graphene degrades the excitonic effects [38–40].

Table 2. The fitting parameters of Tauc-Lorentz and Drude oscillators for monolayer graphene on Si and SiO_2/Si substrates (300 K).

Graphene Samples					
	Tauc-Lorentz	Amp_1 = 108.5431	Br_1 = 1.024	Eo_1 = 0.433 eV	Eg_1 = 0.138 eV
Monolayer on Si	Tauc-Lorentz	Amp_2 = 26.2332	Br_2 = 2.677	Eo_2 = 2.085 eV	Eg_2 = 0.233 eV
	Tauc-Lorentz	Amp_3 = 11.5482	Br_3 = 7.543	Eo_3 = 2.944 eV	Eg_3 = 0 eV
	Tauc-Lorentz	Amp_4 = 7.2054	Br_4 = 1.307	Eo_4 = 4.492 eV	Eg_4 = 0.191 eV
	Tauc-Lorentz	Amp_5 = 14.3884	Br_5 = 0.56	Eo_5 = 4.477 eV	Eg_5 = 0.87 eV
	Drude	Rsisitivity = 0.0008 Ω cm	Scat. Time = 12.576 fs	-	-
	Tauc-Lorentz	Amp_1 = 41.068	Br_1 = 2.783	Eo_1 = 0.329 eV	Eg_1 = 0.174 eV
	Tauc-Lorentz	Amp_2 = 24.0227	Br_1 = 2.783	Eo_2 = 1.799 eV	Eg_2 = 0.188 eV
	Tauc-Lorentz	Amp_3 = 14.095	Br_3 = 3.618	Eo_3 = 3.739 eV	Eg_3 = 0.476 eV
Monolayer on SiO_2/Si	Tauc-Lorentz	Amp_4 = 9.9583	Br_4 = 1.641	Eo_4 = 4.172 eV	Eg_4 = 0.554 eV
	Tauc-Lorentz	Amp_5 = 15.58	Br_5 = 0.904	Eo_5 = 4.594 eV	Eg_4 = 2.077 eV
	Drude	Rsisitivity = 1000 Ω cm	Scat. Time = 1000 fs	-	-

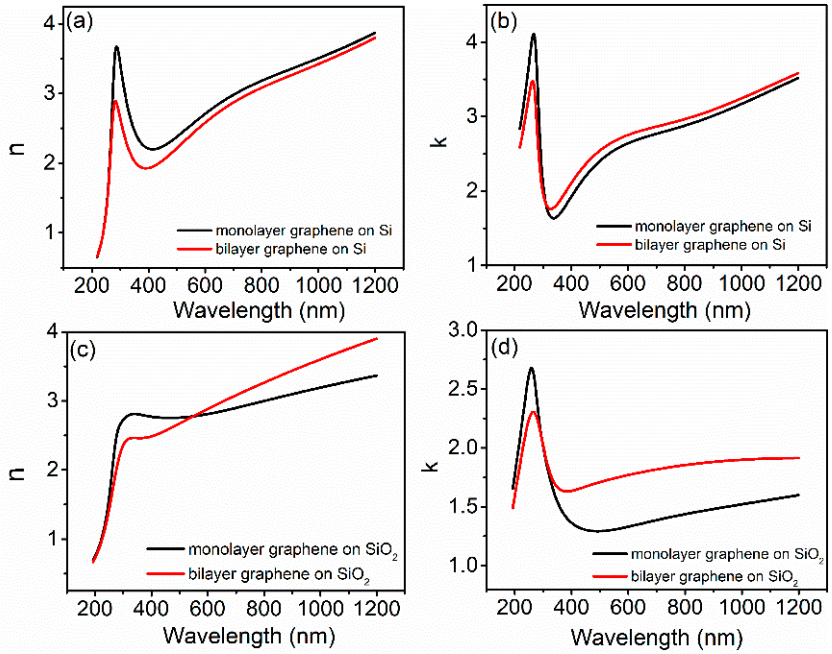

Figure 4. Layer-dependent optical constants of graphene on Si (**a**,**b**) and on SiO_2/Si substrate (**c**,**d**).

In Figure 5 we have displayed the results of temperature-dependent optical constants for two monolayer graphene on Si and SiO_2/Si substrates from 300 K to 500 K with a step of 20 K. The optical constants of monolayer graphene on Si varied consistently with temperature. In the region of λ between 400 to 1200 nm, we noticed the n increased while k decreased with the increase of temperature because the coupling between light and electrons was intensified in graphene. However, the optical constants [n, k] of monolayer graphene on SiO_2/Si exhibited unpredictable variations, i.e., the refractive index n and the extinction coefficient k displayed fluctuations with the increase of temperature.

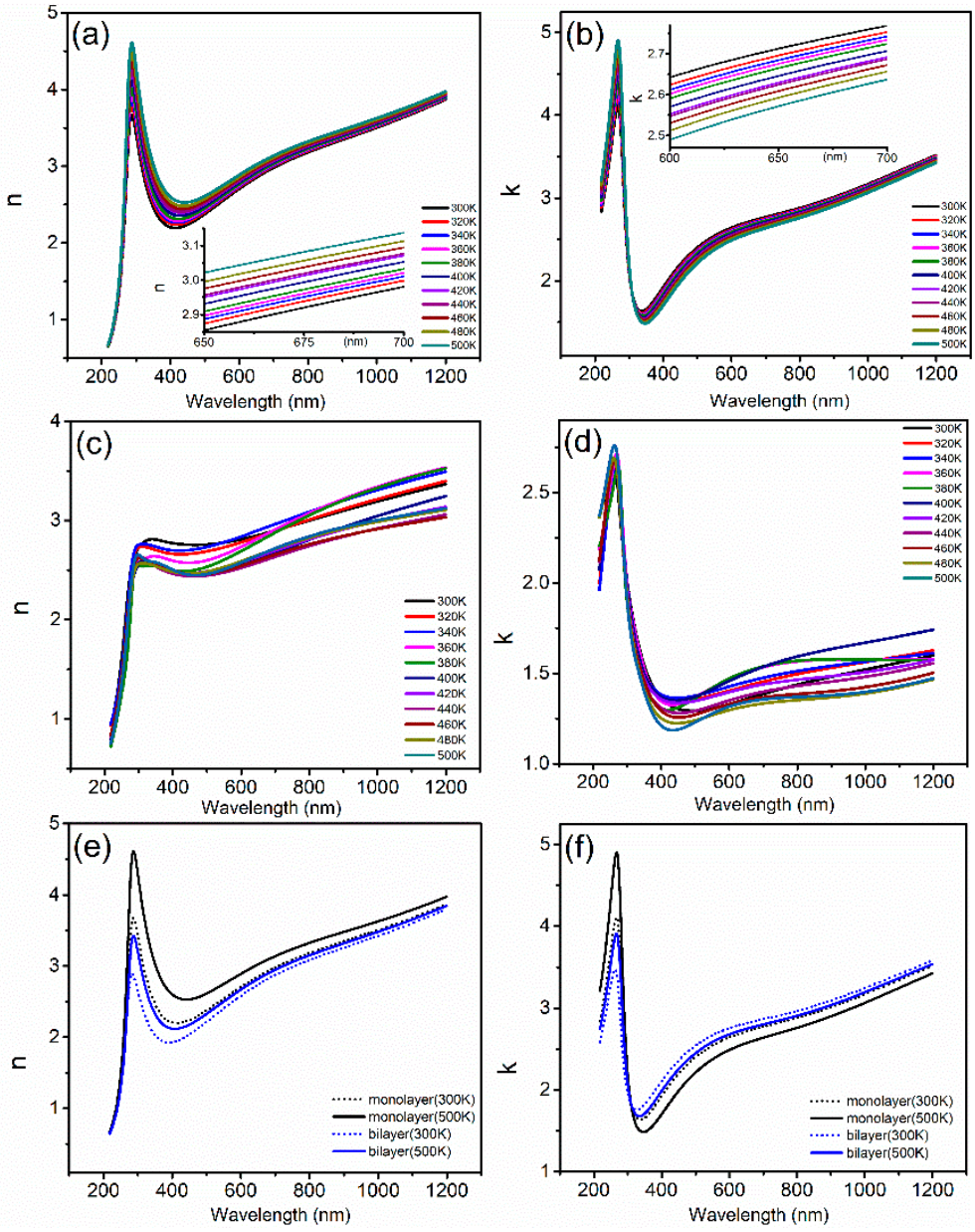

Figure 5. Temperature-dependent optical constants of graphene on Si substrate (**a**,**b**) and on SiO_2/Si substrate (**c**,**d**) from 300 K to 500 K with a step of 20 K. (**e**,**f**) optical constants of four graphene samples on Si at 300 K and at 500 K.

Figure 5e,f illustrates respectively the difference of the extracted optical constants by VASE measurements for four samples of graphene sheets prepared on Si substrate at 300 K and at 500 K. It was revealed that the difference of optical constants between 300 K and 500 K for the monolayer graphene on Si were bigger than those of bilayer graphene, suggesting more temperature sensitivity of the monolayer graphene. It could be caused by the fact that monolayer graphene has more defects, stronger graphene-substrate interactions, and lower thermal stability. The temperature effect was relatively smaller and the thermal stability was enhanced with the increasing number of layers.

Graphene is usually applied in photoelectric devices. The optical constant $n(\lambda)$ reflects the dispersion properties of graphene. It is essential to understand the dependence of dispersion properties of graphene on wavelength and temperature in the transparent region. To further explore the specific dispersion relationship of graphene on Si and on SiO_2/Si substrates, we fitted the n by using a like-Sellmeier equation based on the extracted data

in the wavelength range of λ between 400–1200 nm at room temperature. The traditional Sellmeier equation describing the dispersion is given by [41]:

$$n(\lambda) = [1 + \sum_{j=1} \frac{A_j \lambda^2}{\lambda^2 - B_j}]^{1/2} \quad (1)$$

where λ is the wavelength, A_j and B_j are the fitting parameters, and j is an integer. The fitting results for monolayer and bilayer graphene are displayed in Figure 6. The dispersion curves of graphene on Si were fitted well by a like-Sellmeier equation with j = 1 and for graphene on SiO_2/Si with j = 2. The fitting parameters are recorded in Table 3 and the fitting parameter B_1 was negative which mainly reflected an anomalous dispersion of graphene. It is worth noting that graphene on SiO_2/Si possessed more complex dispersion features. It was possibly caused by an enhancing layer-to-layer interaction which complicated the dispersion relationship.

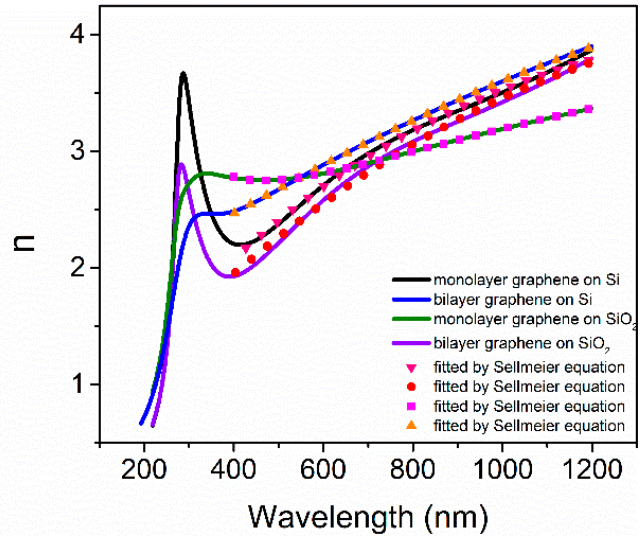

Figure 6. The refractive indices of graphene on Si and on SiO_2/Si substrates fitted by a like-Sellmeier Equation (1) in the wavelength range of 400–1200 nm.

Table 3. Fitting parameters of graphene on Si and on SiO_2/Si substrates by using a like-Sellmeier Equation (1).

Graphene Samples	A_1	B_1 ($\times 10^5$ nm^2)	A_2	B_2 ($\times 10^5$ nm^2)	R^2
monolayer on Si	21.40 ± 0.05	−8.674 ± 0.034	-	-	0.99747
bilayer on Si	24.486 ± 0.124	−12.360 ± 0.095	-	-	0.99418
monolayer on SiO_2	13.682 ± 0.025	−17.006 ± 0.078	3.935 ± 0.006	0.466 ± 0.001	0.99987
bilayer on SiO_2	25.107 ± 0.074	−20.045 ± 0.162	3.713 ± 0.025	−0.238 ± 0.008	0.99992

Furthermore, for graphene on Si substrate, the parameters A_1 and B_1 as a function of temperature (T) were well represented by a polynomial which is given by.

$$\begin{aligned} A_1(T) &= a_0 + a_1 T + a_2 T^2 \\ B_1(T) &= b_0 + b_1 T + b_2 T^2 \end{aligned} \quad (2)$$

where a_0, a_1, a_2, b_0, b_1, and b_2 are constants. By substituting the testing temperature and values of A_1 and B_1 into Equation (2) the fitted results are shown in Figure 7. The red solid lines are the fitted curves using Equation (2), with parameter values of a_0, a_1, a_2, b_0, b_1, and b_2 tabulated in Table 4. Combining the fitting results of expressions (1) and (2), the complete dispersion and temperature-dependent properties of graphene were revealed.

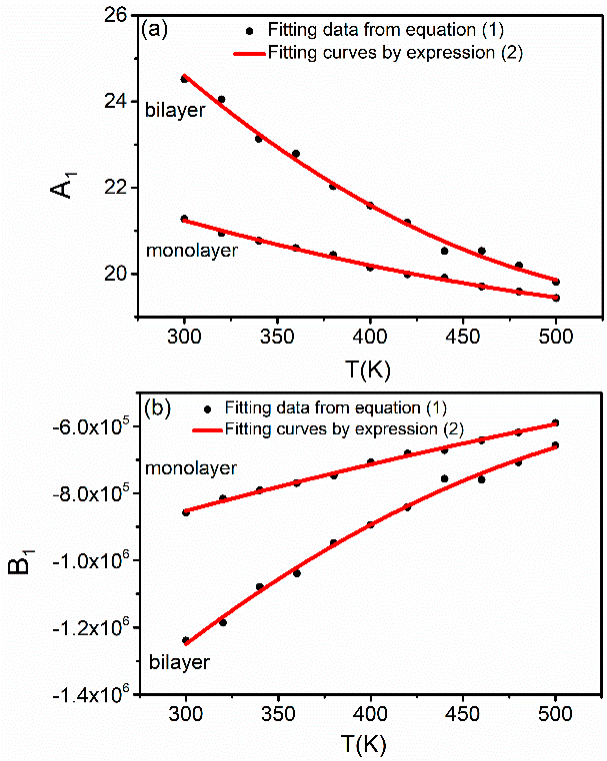

Figure 7. The parameters A_1 and B_1 as a function of temperature from 300 K to 500 K for the graphene on Si substrate.

Table 4. The fitting parameters using Equation (2) for graphene on Si.

Graphene Samples	a_0	a_1	a_2 ($\times 10^{-5}$ K^{-2})	b_0 ($\times 10^6$ nm)	b_1 (10^3 nm^2 K^{-1})	b_2 (nm^2 K^{-2})
monolayer on Si	26.16 ± 0.58	-0.020 ± 0.002	1.495 ± 0.368	-1.379 ± 0.085	2.038 ± 0.430	-0.932 ± 0.530
bilayer on Si	41.302 ± 1.790	-0.074 ± 0.009	6.387 ± 1.136	-3.068 ± 0.228	7.94 ± 1.16	-6.256 ± 1.450

4. Conclusions

In summary, the results of the comprehensive study for the optical properties of graphene revealed interesting characteristics which are not only substrate-, layer- but also temperature-dependent. The graphene samples on Si substrate exhibited significant dispersion features and higher exciton transition energy than those on SiO_2/Si substrate. With the increase of temperatures from 300 K to 500 K, the optical constants of monolayer graphene on Si varies regularly while the monolayer graphene on SiO_2/Si has fluctuations. An experiential formula of a like-Sellmeier expression is demonstrated well exemplifying the wavelength dependence of refractive indices of monolayer and bilayer graphene samples. In addition, for monolayer graphene on Si, the temperature-dependent dispersion properties are well described by combining the like-Sellmeier equation and a quadratic expression.

Author Contributions: Conceptualization, L.W. (Lingyu Wan) and S.W.; Data curation, S.W. and L.W. (Liangmin Wei); Formal analysis, L.W. (Lingyu Wan) and S.W.; Funding acquisition, L.W. (Lingyu Wan); Investigation, L.W. (Lingyu Wan), S.W. and Z.F.; Project administration, L.W. (Lingyu Wan); Resources, L.W. (Lingyu Wan), K.H. and Z.F.; Supervision, L.W. (Lingyu Wan); Writing—original draft, L.W. (Lingyu Wan) and S.W.; Writing—review & editing, L.W. (Lingyu Wan), D.N.T. and Z.F. All authors have read and agreed to the published version of the manuscript.

Funding: This research was funded by the Guangxi Natural Science Foundation, China (2018GXNSFAA138127).

Conflicts of Interest: The authors declare no conflict of interest.

References

1. Novoselov, K.S.; Geim, A.K.; Morozov, S.V.; Jiang, D.; Zhang, Y.; Dubonos, S.V.; Grigorieva, I.V.; Firsov, A.A. Electric Field Effect in Atomically Thin Carbon Films. *Science* **2004**, *306*, 666–669. [CrossRef]
2. Novoselov, K.S.; Geim, A.K.; Morozov, S.V.; Jiang, D.; Katsnelson, M.I.; Grigorieva, I.V.; Dubonos, S.V.; Firsov, A.A. Two-dimensional gas of massless Dirac fermions in graphene. *Nature* **2005**, *438*, 197–200. [CrossRef]
3. Geim, A.K.; Novoselov, K.S. The rise of graphene. *Nat. Mater.* **2007**, *6*, 183–191. [CrossRef] [PubMed]
4. Balandin, A.A.; Ghosh, S.; Bao, W.Z.; Calizo, I.; Teweldebrhan, D.; Miao, F.; Lau, C.N. Superior Thermal Conductivity of Single-Layer Graphene. *Nano Lett.* **2008**, *8*, 902–907. [CrossRef]
5. Lee, C.; Wei, X.; Kysar, J.W.; Hone, J. Measurement of the Elastic Properties and Intrinsic Strength of Monolayer Graphene. *Science* **2008**, *321*, 385–388. [CrossRef]
6. Novoselov, K.S.; Jiang, Z.; Zhang, Y.; Morozov, S.V.; Stormer, H.L.; Zeitler, U. Room-Temperature Quantum Hall Effect in Graphene. *Science* **2007**, *315*, 1379. [CrossRef]
7. Wu, F.C.; Hwang, E.; Das Sarma, S. Phonon-induced giant linear-in-T resistivity in magic angle twisted bilayer graphene: Ordinary strangeness and exotic superconductivity. *Phys. Rev. B* **2019**, *99*, 165112. [CrossRef]
8. Lu, X.B.; Stepanov, P.; Yang, W.; Xie, M.; Aamir, M.A.; Das, I.; Urgell, C.; Watanabe, K.; Taniguchi, T.; Zhang, G.Y.; et al. Superconductors, orbital magnets and correlated states in magic-angle bilayer graphene. *Nature* **2019**, *574*, 653–657. [CrossRef] [PubMed]
9. Nair, R.R.; Blake, P.; Grigorenko, A.N.; Novoselov, K.S.; Booth, T.J.; Stauber, T.; Peres, N.M.R.; Geim, A.K. Fine Structure Constant Defines Visual Transparency of Graphene. *Science* **2008**, *320*, 1308. [CrossRef]
10. Wang, X.F.; Chen, Y.P.; Nolte, D.D. Strong anomalous optical dispersion of graphene: Complex refractive index measured by Picometrology. *Opt. Express* **2008**, *16*, 22105–22112. [CrossRef]
11. Kravets, V.G.; Grigorenko, A.N.; Nair, R.R.; Blake, P.; Anissimova, S.; Novoselov, K.S.; Geim, A.K. Spectroscopic ellipsometry of graphene and an exciton-shifted van Hove peak in absorption. *Phys. Rev. B* **2010**, *81*, 115413. [CrossRef]
12. Wurstbauer, U.; Roling, C.; Wurstbauer, U.; Wegscheider, W.; Vaupel, M.; Thiesen, P.H.; Weiss, D. Imaging ellipsometry of graphene. *Appl. Phys. Lett.* **2010**, *97*, 231901. [CrossRef]
13. Weber, J.W.; Calado, V.E.; van de Sanden, M.C.M. Optical constants of graphene measured by spectroscopic ellipsometry. *Appl. Phys. Lett.* **2010**, *97*, 091904. [CrossRef]
14. Nelson, F.J.; Kamineni, V.K.; Zhang, T.; Comfort, E.S.; Lee, J.U.; Diebold, A.C. Optical properties of large-area polycrystalline chemical vapor deposited graphene by spectroscopic ellipsometry. *Appl. Phys. Lett.* **2010**, *97*, 253110. [CrossRef]
15. Isić, G.; Jakovljević, M.; Filipović, M.; Jovanović, D.; Vasić, B.; Lazović, S.; Puač, N.; Petrović, Z.L.; Kostić, R.; Gajić, R.; et al. Spectroscopic ellipsometry of few-layer graphene. *J. Nanophotonics* **2011**, *5*, 051809. [CrossRef]
16. Losurdo, M.; Giangregorio, M.M.; Capezzuto, P.; Bruno, G. Ellipsometry as a Real-Time Optical Tool for Monitoring and Understanding Graphene Growth on Metals. *J. Phys. Chem. C* **2011**, *115*, 21804–21812. [CrossRef]
17. Kostruba, A.M. Influence of the graphene substrate on morphology of the gold thin film. Spectroscopic ellipsometry study. *Appl. Surf. Sci.* **2013**, *283*, 603–611. [CrossRef]
18. Matković, A.; Ralević, U.; Chhikara, M.; Jakovljević, M.M.; Jovanović, D.; Bratina, G.; Gajić, R. Influence of transfer residue on the optical properties of chemical vapor deposited graphene investigated through spectroscopic ellipsometry. *J. Appl. Phys.* **2013**, *114*, 93505. [CrossRef]
19. Shen, C.C.; Tseng, C.C.; Lin, C.T.; Li, L.J.; Liu, H.L. Optical properties of nitrogen-doped graphene thin films probed by spectroscopic ellipsometry. *Thin. Solid. Films* **2014**, *571*, 675–679. [CrossRef]
20. Chang, Y.-C.; Liu, C.-H.; Liu, C.-H.; Zhong, Z.; Norris, T.B. Extracting the complex optical conductivity of mono- and bilayer graphene by ellipsometry. *Appl. Phys. Lett.* **2014**, *104*, 261909. [CrossRef]
21. Ochoa-Martínez, E.; Gabás, M.; Barrutia, L.; Pesquera, A.; Centeno, A.; Palanco, S.; Zurutuza, A.; Algora, C. Determination of refractive index and extinction coefficient of standard production CVD-graphene. *Nanoscale* **2015**, *7*, 1491–1500. [CrossRef] [PubMed]
22. Li, W.; Cheng, G.; Liang, Y.; Tian, B.; Liang, X.; Peng, L.; Hight Walker, A.R.; Gundlach, D.J.; Nguyen, N.V. Broadband optical properties of graphene by spectroscopic ellipsometry. *Carbon* **2016**, *99*, 348–353. [CrossRef]
23. Pápa, Z.; Csontos, J.; Smausz, T.; Toth, Z.; Budai, J. Spectroscopic ellipsometric investigation of graphene and thin carbon films from the point of view of depolarization effects. *Appl. Surf. Sci.* **2017**, *421*, 714–721. [CrossRef]
24. Song, B.K.; Gu, H.G.; Zhu, S.M.; Jiang, H.; Chen, X.G.; Zhang, C.W.; Liu, S.Y. Broadband optical properties of graphene and HOPG investigated by spectroscopic Mueller matrix ellipsometry. *Appl. Surf. Sci.* **2018**, *439*, 1079–1087. [CrossRef]
25. Castriota, M.; Politano, G.G.; Vena, C.; De Santo, M.P.; Desiderio, G.; Davoli, M.; Cazzanelli, E.; Versace, C. Variable Angle Spectroscopic Ellipsometry investigation of CVD-grown monolayer graphene. *Appl. Surf. Sci.* **2019**, *467*, 213–220. [CrossRef]
26. Sun, D.; Wu, Z.K.; Divin, C.; Li, X.B.; Berger, C.; de Heer, W.A.; First, P.N.; Norris, T.B. Ultrafast Relaxation of Excited Dirac Fermions in Epitaxial Graphene. Using Optical Differential Transmission Spectroscopy. *Phys. Rev. Lett.* **2008**, *101*, 157402. [CrossRef] [PubMed]
27. Zhu, S.E.; Yuan, S.J.; Janssen, G.C.A.M. Optical transmittance of multilayer graphene. *Europhys. Lett.* **2012**, *108*, 17007. [CrossRef]

28. Zhou, S.Y.; Gweon, G.H.; Fedorov, A.V.; First, P.N.; De Heer, W.A.; Lee, D.H.; Guinea, F.; Castro Neto, A.H.; Lanzara, A. Substrate induced bandgap opening in epitaxial graphene. *Nat. Mater.* **2007**, *6*, 770–775. [CrossRef] [PubMed]
29. Peng, X.Y.; Ahuja, R. Symmetry breaking induced bandgap in epitaxial graphene layers on SiC. *Nano Lett.* **2008**, *8*, 4464–4468. [CrossRef] [PubMed]
30. Tiwari, R.P.; Stround, D. Tunable band gap in graphene with a noncentrosymmetric superlattice potencial. *Phys. Rev. B* **2009**, *79*, 205435. [CrossRef]
31. Azadeh, M.S.S.; Kokabi, A.; Hosseini, M.; Fardmanesh, M. Tunable bandgap opening in the proposed structure of silicon-doped graphene. *Micro Nano Lett.* **2011**, *6*, 582–585. [CrossRef]
32. Das, A.; Chakraborty, B.; Sood, A.K. Raman spectroscopy of graphene on different substrates and influence of defect. *Bull. Mater. Sci.* **2008**, *31*, 579–584. [CrossRef]
33. Cancado, L.G.; Jorio, A.; Ferreira, E.H.M.; Stavale, F.; Achete, C.A.; Capaz, R.B.; Moutinho, M.V.O.; Lombardo, A.; Kulmala, T.S.; Ferrari, A.C. Quantifying Defects in Graphene via Raman Spectroscopy at Different Excitation Energies. *Nano* **2011**, *11*, 3190–3196. [CrossRef]
34. Eckmann, A.; Felten, A.; Verzhbitskiy, I.; Davey, R.; Casiraghi, C. Raman study on defective graphene: Effect of the excitation energy, type, and amount of defects. *Phys. Rev. B* **2013**, *88*, 035426. [CrossRef]
35. Enzo, C.; Oreste, D.L.; Danilo, V.; Alfonso, P.; Marco, C.; Giovanni, D.; Penelope, D.S.M.; Alfredo, A.; Angela, F.; Tania, R.; et al. Characterization of graphene grown on copper foil by chemical vapor deposition (CVD) at ambient pressure conditions. *J. Raman Spectrosc.* **2018**, *49*, 1006–1014.
36. Li, B.B.; Yu, D.P.; Zhang, S.L. Raman spectral study of silicon nanowires. *Phys. Rev. B* **1999**, *59*, 1645–1648. [CrossRef]
37. Tan, P.H.; An, L.; Liu, L.Q.; Guo, Z.X.; Czerw, R.; Carroll, D.L.; Ajayan, P.M.; Zhang, N.; Guo, H.L. Probing the phonon dispersion relations of graphite from the double-resonance process of Stokes and anti Stokes Raman scatterings in multiwalled carbon nanotubes. *Phys. Rev. B* **2002**, *66*, 245410. [CrossRef]
38. Mak, K.F.; Shan, J.; Heinz, T.F. Seeing Many-Body Effects in Single- and Few-Layer Graphene: Observation of Two-Dimensional Saddle-Point Excitons. *Phys. Rev. Lett.* **2011**, *106*, 046401. [CrossRef]
39. Yang, L.; Deslippe, J.; Park, C.-H.; Cohen, M.L.; Louie, S.G. Excitonic Effects on the Optical Response of Graphene and Bilayer Graphene. *Phys. Rev. Lett.* **2009**, *103*, 186802. [CrossRef] [PubMed]
40. Chae, D.-H.; Utikal, T.; Weisenburger, S.; Giessen, H.; von Klitzing, K.; Lippitz, M.; Smet, J. Excitonic Fano Resonance in Free-Standing Graphene. *Nano Lett.* **2011**, *11*, 1379–1382. [CrossRef] [PubMed]
41. Tropf, W.J. Temperature-dependent refractive index models for BaF2, CaF2, MgF2, SrF2, LiF, NaF, KCI, ZnS, and ZnSe. *Opt. Eng.* **1995**, *34*, 1369–1373. [CrossRef]